

Article

Density Functional Theory Study of the Hydrogenation of Carbon Monoxide over the Co (001) Surface: Implications for the Fischer–Tropsch Process

Mostafa Torkashvand¹, Saeedeh Sarabadani Tafreshi^{1,*}  and Nora H. de Leeuw^{2,3,*} 

¹ Department of Chemistry, Amirkabir University of Technology, No. 350, Hafez Avenue, Valiasr Square, Tehran 1591634311, Iran

² School of Chemistry, University of Leeds, Leeds LT2 9JT, UK

³ Department of Earth Sciences, Utrecht University, 3584 CB Utrecht, The Netherlands

* Correspondence: s.s.tafreshi@aut.ac.ir (S.S.T.); n.h.deleeuw@leeds.ac.uk (N.H.d.L.)

Abstract: The increasing demand for renewable fuels and sustainable products has encouraged growing interest in the development of active and selective catalysts for the conversion of carbon monoxide into desirable products. The Fischer–Tropsch process consists of the reaction of a synthesis gas mixture containing carbon monoxide and hydrogen (syngas), which are polymerized into liquid hydrocarbon chains, often using a cobalt catalyst. Here, first-principles calculations based on the density functional theory (DFT) are used to investigate the reaction mechanism of the Fischer–Tropsch synthesis over the Co (001) surface. The most energetically favorable adsorption configurations of the species involved in the carbon monoxide hydrogenation process are identified, and the possible elementary steps of hydrogenation and their related transition states are explored using the Vienna Ab initio simulation package (VASP). The results provide the mechanisms for the formation of CH₄, CH₃OH and C₂H₂ compounds, where the calculations suggest that CH₄ is the dominant product. Findings from the reaction energies reveal that the preferred mechanism for the hydrogenation of carbon monoxide is through HCO and cis-HCOH, and the largest exothermic reaction energy in the CH₄ formation pathway is released during the hydrogenation of cis-HCOH (−0.773 eV). An analysis of the kinetics of the hydrogenation reactions indicates that the CH production from cis-HCOH has the lowest energy barrier of just 0.066 eV, and the hydrogenation of CO to COH, with the largest energy barrier of 1.804 eV, is the least favored reaction kinetically.

Keywords: DFT; carbon monoxide; Fischer–Tropsch Synthesis; cobalt catalyst; CH₄



Citation: Torkashvand, M.; Sarabadani Tafreshi, S.; de Leeuw, N.H. Density Functional Theory Study of the Hydrogenation of Carbon Monoxide over the Co (001) Surface: Implications for the Fischer–Tropsch Process. *Catalysts* **2023**, *13*, 837. <https://doi.org/10.3390/catal13050837>

Academic Editors: Antonia Iazzetti and Alessia Ciogli

Received: 18 March 2023

Revised: 9 April 2023

Accepted: 14 April 2023

Published: 4 May 2023



Copyright: © 2023 by the authors. Licensee MDPI, Basel, Switzerland. This article is an open access article distributed under the terms and conditions of the Creative Commons Attribution (CC BY) license (<https://creativecommons.org/licenses/by/4.0/>).

1. Introduction

Carbon monoxide (CO) is a colorless, odorless and non-irritable gas [1,2]. With a specific gravity of 0.97, CO is slightly lighter than air and is mainly produced by the incomplete combustion of organic compounds [3–6]. Fischer–Tropsch synthesis [7–9] (FTS) is a process that has been used for many decades as it gives access to industrially important chemicals from CO [10–13]. As the products of FTS are a complex mixture of a wide range of organic compounds, selectivity toward desired products is the most important issue in this reaction [14]. In recent years, there has been an increasing motivation to deploy FTS at commercial scales, which has fueled the search for high-performance catalysts [15].

Several catalysts have been examined for their potential to catalyze CO hydrogenation [16–19]. The rate of formation and the selectivity towards certain hydrocarbons are the key challenges in FTS and they depend on the catalyst used [20]. Transition metal catalysis has long been recognized as a reliable and modular means of constructing complex molecules from simple, readily accessible starting materials [21].

Many studies based on density functional theory (DFT) calculations of FTS synthesis over metallic surfaces have been reported in the literature [22–30]. For example,

Zhang et al. [31] studied the hydrogenation mechanism of carbon dioxide and carbon monoxide over Ru(0001), where they found that during CO hydrogenation, CO may dissociate via either a COH or CHO intermediate, resulting in C and CH species, respectively [31]. A broad array of palladium catalytic systems, mainly based on Pd salts and complexes in the presence of a base, are currently employed as efficient, chemoselective and productive homogeneous or heterogeneous catalysts to promote C–C cross-coupling reactions [12,32–42]. The suppression of methane production through optimization of the physical properties of Fe has allowed Hirsu and co-workers to further understand and develop the performance of iron-based catalysts [43]. Iron has a high water–gas shift activity and is therefore suitable for syngas feedstocks of a low H₂/CO ratio, such as those derived from coal gasification [44].

Cobalt is generally preferred over Fe and Ru for FTS as it possesses high activity and selectivity in the production of long-chain hydrocarbons from syngas [45–48]. Ge et al. [30] reported a density functional theory study which was used to analyze the first steps in the mechanism of Fischer–Tropsch synthesis, i.e., CO adsorption and activation over the close-packed {0001}, corrugated {1120} and stepped {1012} and {1124} Co surfaces. The adsorption energy of CO tends to increase as the CO coverage is reduced. If chemisorbed CO is used as the reference state, the reaction on Co {0001} and {1120} becomes endothermic whereas it remains exothermic on Co {1012} and {1124}. On Co {1012} and {1124}, low-coverage pathways with activation energies that lie below the energy of gas-phase CO were identified. The existence of these low-energy pathways on the stepped surfaces allows a CO molecule from the gas phase to dissociate spontaneously [30]. The elementary step from C₂ to C₆ and the α -olefin selectivity through the hydrogenation and dehydrogenation of n-alkyl groups on Co (0001) have been investigated in an early work by Cheng et al. [22] In another study, Cheng et al. studied CO hydrogenation on fcc Co (111), where they sought to study the formation of C₂ hydrocarbons on the surfaces of fcc Co, with significant results for the adsorption energies and activation energies [48]. Petersen et al. investigated CO dissociation at step and kink sites on fcc Co (221) and Co (321) surfaces. In both cases, the direct CO dissociation path yields the lowest overall activation energy for CO dissociation, with H-assisted routes via HCO or COH intermediates being higher in energy [49]. Helden et al. reported DFT results from a comparative study of the direct and hydrogen-assisted CO dissociation pathways on the surface of fcc Co (100) [50,51], where they clearly showed that the hydrogen-assisted CO dissociation mechanism is an important contributor to the CO activation mechanism during the first step of FTS [51].

To the best of our knowledge, there is no comprehensive theoretical investigation of CO hydrogenation via FTS synthesis on the fcc Co (001) surface. As such, this paper presents the results of a DFT study of the CO hydrogenation mechanism and the reaction and activation energies towards different products [52,53], confirming that CH₄ is the main product, both thermodynamically and kinetically [54].

2. Results and Discussion

2.1. Thermodynamic Analysis

2.1.1. Adsorption of Molecules

All molecule structures were downloaded from PubChem [55–57] at the National Center for Biotechnology Information [58]. They were then edited and designed through Materials Studio [59], VESTA [60], and P4vasp [61,62].

In this section, the adsorption of a range of intermediates on the Co (001) surface is examined. As illustrated in Figure 1, there are three different positions for the adsorption of molecules on the surface, i.e., the bridge, hollow and top sites.

The preferred adsorption positions for all intermediates on the Co (001) surface are presented in Figure 2, with geometric information and adsorption energies calculated using Equation (3), provided in Table 1. More information on the structural details of

the adsorption geometries are found in Table S1 and Figure S1 of the Supplementary Information.

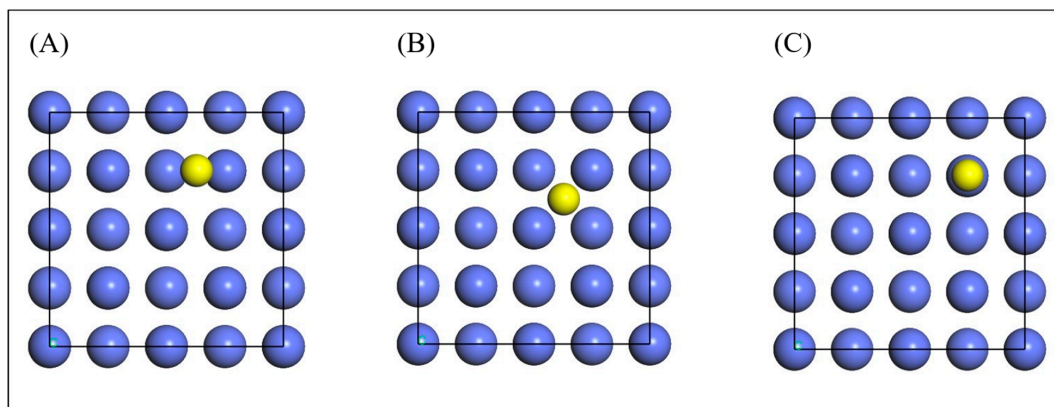


Figure 1. Three different positions for adsorption of molecules on Co (001) surface. (A) Bridge, (B) hollow, and (C) top.

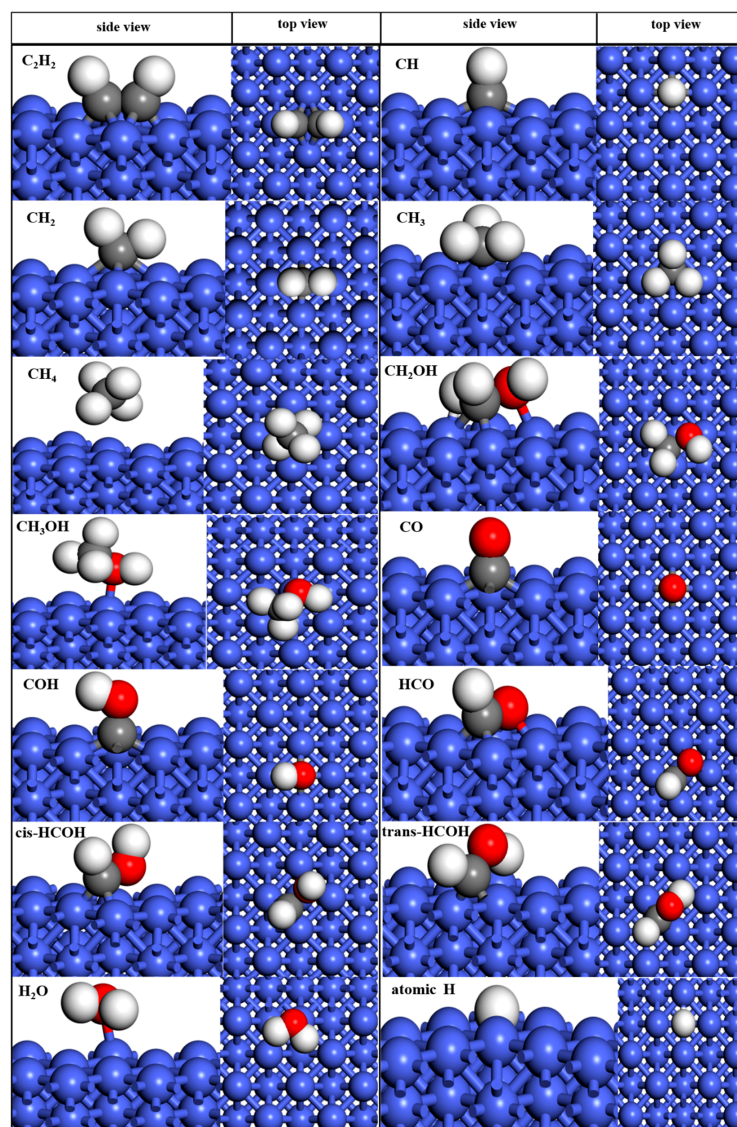


Figure 2. The adsorption geometries of the studied molecules during CO hydrogenation on the Co (001) surface.

All possible adsorption configurations were studied, and the lowest-energy adsorption geometry for each intermediate was selected as the final configuration. The results show that the preferred site for adsorption is the hollow site, although some molecules adsorb on top, and just one adsorbs on a bridge site. In addition, the results show that all molecules prefer to interact with the surface through their carbon atom.

CO binds to the Co (001) surface through its C atom, which is located exactly in the hollow site between surface Co atoms, with a Co–C bond length of 2.03 Å and an adsorption energy of -2.268 eV. The negative value of the adsorption energy indicates that the adsorption is an exothermic process. This value is in good agreement with the literature values for the adsorption of CO [63–66].

COH adsorbs vertically and binds to the Co (001) surface through its C atom, with a Co–C bond length of 1.960 Å and an adsorption energy of -5.696 eV. This mode of adsorption is similar to that found by Psfogiannakis et al. on the Pt (111) surface [63], where COH is also adsorbed in a hollow site with a calculated adsorption energy of -5.64 eV.

When the HCO molecule is adsorbed, two oxygen and carbon atoms bind strongly to the surface atoms, with Co–O and Co–C bond lengths of 1.928 and 1.917 Å, respectively, while its hydrogen atom does not interact with the surface; the adsorption energy for this molecule is -4.03 eV.

Cis- and trans-HCOH are adsorbed with similar energies of -3.919 and -3.583 eV, respectively. Cis-HCOH adsorbs at a hollow position, while trans-HCOH is located exactly on a bridge position between two cobalt atoms. Another difference between the adsorption geometries of these two species is their binding to the surface, as cis-HCOH bonds to the cobalt surface atom through both its carbon and oxygen atoms, with Co–C and Co–O bond lengths of 1.970 and 2.365 Å, respectively, while trans-HCOH binds to the surface only through its carbon atom, with a Co–C bond length of 1.930 Å.

CH, CH₂, CH₃ and CH₄ adsorb at the hollow position on the Co surface, with the former three species binding to the Co (001) surface through their carbon atoms with bond lengths of 1.942, 2.091, and 1.967 Å, respectively. The CH₄ molecule approaches the surface via its C and H atoms, at average distances of 3.645 and 2.841 Å, respectively. The adsorption energies for CH, CH₂, CH₃ and CH₄ were calculated at -7.964 , -5.611 , -2.972 and -0.204 eV, respectively. For comparison, the adsorption energies of CH and CH₂ on the Pt (111) surface were calculated by Psfogiannakis et al. at -7.55 and -4.56 eV, respectively, whereas the adsorption of CH₃ at the surface was calculated at -2.40 eV [63], and the adsorption energy for CH₄ on the Ru (0001) surface was calculated at -0.17 eV by Zhang et al. [31].

H₂O adsorbs on top of a surface Co atom on the Co (001) surface via its oxygen atom, with an adsorption energy of -0.746 eV, forming a Co–O bond length of 2.141 Å. CH₂OH prefers to be sited in a hollow position between four surface Co atoms, where it binds by its oxygen and carbon atoms with Co–O and Co–C bond lengths of 2.110 and 1.941 Å and an adsorption energy of -2.74 eV. While Ashwell et al. [64] reported an energy of -1.68 eV for CH₂OH adsorption on the Ni (110) surface, Psfogiannakis et al. calculated adsorption energies that were more similar to our result, obtaining -2.79 eV [63] as the adsorption energy of CH₂OH on the Pt (111) surface.

The oxygen atom of CH₃OH adsorbs above a surface Co atom, with an adsorption energy of just -0.718 eV, and forms a Co–O bond with a bond length of 2.117 Å. The adsorption geometry of C₂H₂ shows that it adsorbs in a hollow site parallel to the surface by bonding to cobalt surface atoms, with a Co–C bond length of 1.343 Å and an adsorption energy of -3.241 eV; this is similar to the adsorption energy of C₂H₂ on the Ni (111) surface, calculated by Medlin and Allendorf to be approximately -2.957 eV [67].

The adsorption energies of the studied intermediates on the Co (001) surface decrease in the order: CH > COH > CH₂ > HCO > cis-HCOH > trans-HCOH > C₂H₂ > CH₃ > CH₂OH > CO > H₂O > CH₃OH > CH₄.

Table 1. The preferred adsorption geometries and energies for all intermediates on the Co (001) surface.

Species	Site, Atom, Bond Length (Å)	E _{ads} (eV)	E _{ads} in Literature (eV)
CO	hollow, carbon, 2.03	−2.268	−2.34(Pt(111)) [63], −1.91 (Ni(110)) [64], −2.00 (Fe(100)) [65], −1.92 (Ni(111)) [66]
COH	hollow, carbon, 1.960	−5.696	−5.64(Pt(111)) [63], −4.01 (Ni(110)) [64], −6.21(Fe(100)) [65],
HCO	hollow, carbon, 1.917	−4.03	−2.60 (Ni(110)) [64], −6.49 (Fe(100)) [65]
Cis-HCOH	hollow, carbon, 1.970	−3.919	−3.51 (Ni(110)) [64], −4.04 (Fe(100)) [65]
Trans-HCOH	bridge, carbon, 1.930	−3.583	−3.25 Ni(110) [64], −4.04 (Fe(100)) [65]
CH	hollow, carbon, 1.942	−7.946	−6.43 (Ni(111)) [66], −7.55(Pt(111)) [63]
CH ₂	hollow, carbon, 2.091	−5.611	−4.01 (Ni(111)) [66], −4.56(Pt(111)) [63]
CH ₃	hollow, carbon, 1.967	−2.972	−2.40(Pt(111)) [63]
CH ₄	hollow, carbon, 3.645	−0.204	−0.17 (Ru(0001)) [31]
H ₂ O	top, oxygen, 2.141	−0.746	−0.29 (Ni(111)) [66]
CH ₂ OH	hollow, oxygen, 2.110 carbon, 1.941	−2.74	−2.79(Pt(111)) [63], −1.68 (Ni(110)) [64]
CH ₃ OH	top, oxygen, 2.117	−0.718	−0.45 (Ni(110)) [64]
C ₂ H ₂	hollow, carbon, 1.843	−3.241	−2.957 (Ni(111)) [67]

2.1.2. Hydrogenation

The hydrogenation of CO is the main goal of this study, and it is also an inseparable part of FTS. After calculating the adsorption of all relevant molecules at the Co (001) surface, we next introduced hydrogen on the surface near the adsorbed molecules to investigate the hydrogenation reactions. Due to the number of possible relative positions for the hydrogen atoms and molecules, several calculations were carried out to identify the lowest-energy positions for hydrogen in each adsorption configuration. The most stable co-adsorbed geometries of each intermediate and H are shown in Figure 3.

The hydrogenation of CO to obtain CH₃OH, CH₄, and C₂H₂ goes first through COH and HCO, followed by the further hydrogenation of these intermediates to form cis-HCOH and trans-HCOH. In the next step, the hydrogenation of cis-HCOH and trans-HCOH can produce either CH₂OH or CH + H₂O, followed by the production of methanol CH₃OH from CH₂OH + H. Finally, CH₄ is produced through three intermediates: CH + H, CH₂ + H, and CH₃ + H.

2.1.3. Reactions

In this section, the reactions underpinning the mechanism of CO hydrogenation on the Co (001) surface are discussed. The reaction energies calculated via Equation (4) are presented in Table 2.

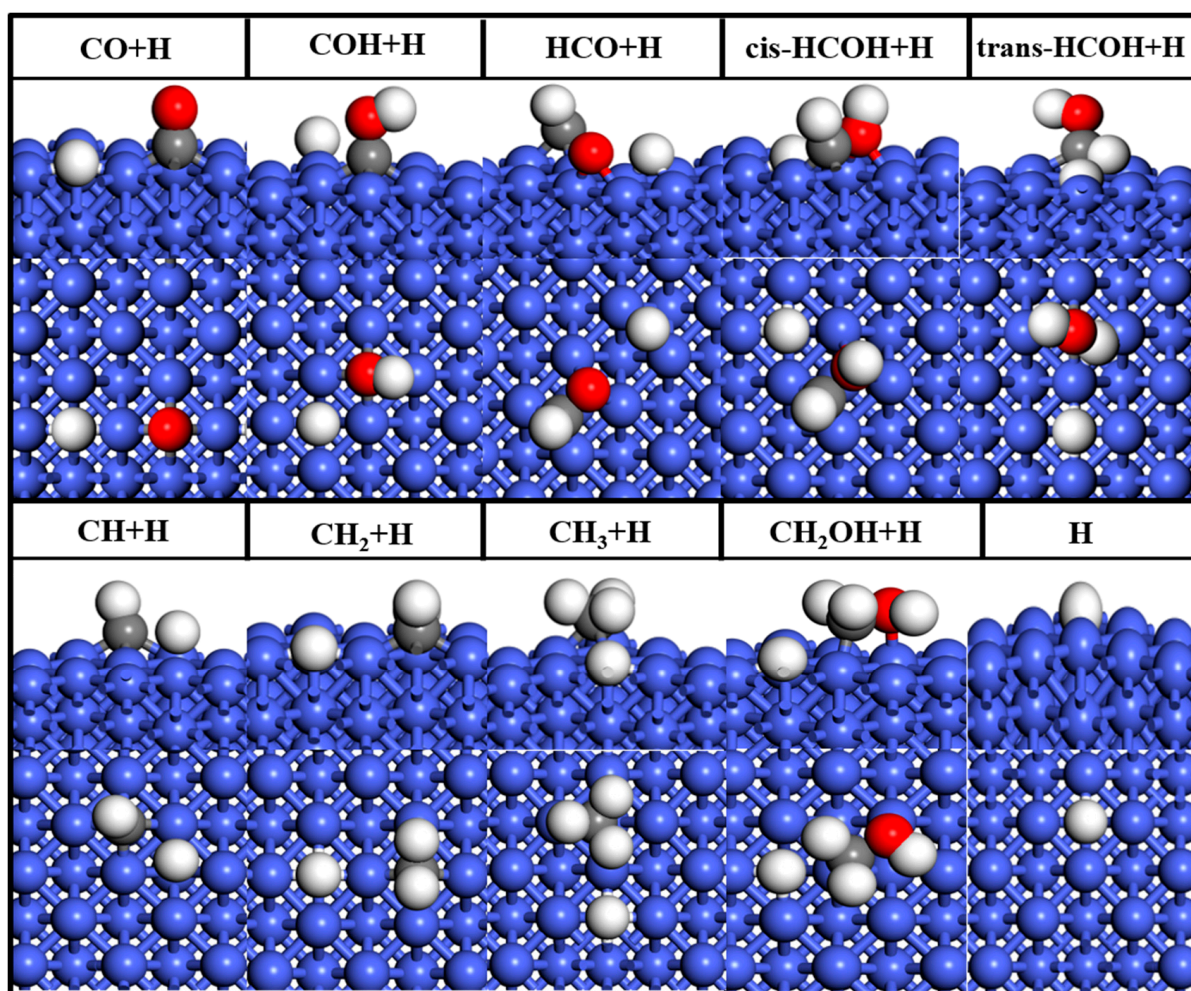


Figure 3. Side views of the lowest-energy co-adsorption configurations of each intermediate and H on Co (001) surface. The gray, white, red, and blue balls represent carbon, hydrogen, oxygen, and cobalt atoms, respectively.

The transformation from CO to form HCO has a reaction energy of about 0.3 eV less than the reaction energy needed to form COH, with the reaction energy for $\text{CO} + \text{H} \rightarrow \text{COH}$ calculated at 0.853 eV. This is in perfect agreement with the work by Zhang et al. [68], who obtained a reaction energy of 0.85 eV to produce COH from the hydrogenation of CO over the InZr_3 surface. The other intermediate produced from the reaction between CO and H is HCO, with the reaction of $\text{CO} + \text{H} \rightarrow \text{HCO}$ requiring an energy of 0.574 eV to proceed. Hirunsit [69] reported a reaction energy of about 0.53 eV for the same reaction, which is very close to our result.

Following this initial CO hydrogenation, both COH and HCO can react with hydrogen, which results in two different isomers of HCOH. The reaction energies of $\text{COH} + \text{H} \rightarrow \text{cis-HCOH}$ and $\text{COH} + \text{H} \rightarrow \text{trans-HCOH}$ are 0.858 and 1.004 eV, respectively, whereas the reaction energies for $\text{HCO} + \text{H} \rightarrow \text{cis-HCOH}$ and $\text{HCO} + \text{H} \rightarrow \text{trans-HCOH}$ differ by 0.2 eV, i.e., to produce cis-HCOH from HCO by $\text{HCO} + \text{H} \rightarrow \text{cis-HCOH}$, the reaction energy is 1.393 eV, while it is 1.539 eV for the reaction $\text{HCO} + \text{H} \rightarrow \text{trans-HCOH}$. The migration of H to the nearby HCOH isomers can lead to either HCOH hydrogenation to form CH_2OH or HCOH dissociation to form CH and H_2O . The former reactions, from either $\text{cis-HCCOH} + \text{H} \rightarrow \text{CH}_2\text{OH}$ or $\text{trans-HCCOH} + \text{H} \rightarrow \text{CH}_2\text{OH}$, have reaction energies of 0.39 eV and -0.12 eV, respectively, while the dissociation reactions of $\text{cis-HCCOH} + \text{H} \rightarrow \text{CH} + \text{H}_2\text{O}$ and $\text{trans-HCCOH} + \text{H} \rightarrow \text{CH} + \text{H}_2\text{O}$ are exothermic, with reaction energies of -0.773 and -1.283 eV, respectively.

After the steps above, there are three ways to reach the desired products; first, the hydrogenation of CH_2OH to CH_3OH , second, a reaction between two CH species to produce acetylene (C_2H_2), and finally, the production of CH_4 through a three-step hydrogenation reaction of $\text{CH} \rightarrow \text{CH}_2 \rightarrow \text{CH}_3 \rightarrow \text{CH}_4$. These three steps consist of the reactions: $\text{CH} + \text{H} \rightarrow \text{CH}_2$, $\text{CH}_2 + \text{H} \rightarrow \text{CH}_3$ and $\text{CH}_3 + \text{H} \rightarrow \text{CH}_4$. The hydrogenation of $\text{CH}_2\text{OH} + \text{H} \rightarrow \text{CH}_3\text{OH}$ has a calculated reaction energy of 0.089 eV compared to Ashwell et al. [64], who calculated the reaction energy for this reaction to be 0.49 eV on the Cu (111) surface. Acetylene is produced by the reaction $\text{CH} + \text{CH}$, with an energy of 1.511 eV. The three-step process to produce CH_4 requires reaction energies for $\text{CH} + \text{H} \rightarrow \text{CH}_2$, $\text{CH} + \text{H} \rightarrow \text{CH}_3$ and $\text{CH} + \text{H} \rightarrow \text{CH}_4$ of 0.019, 0.679, and 0.491 eV, respectively.

In the above-described network of reactions, all reactions except three are endothermic. The transformation of $\text{cis-HCOH} + \text{H}$ to $\text{CH} + \text{H}_2\text{O}$ is exothermic, with a reaction energy of -0.773 eV, whereas the other two exothermic reactions are the result of trans-HCOH hydrogenation, with reaction energies of -0.120 eV and -1.283 eV to produce CH_2OH and $\text{CH} + \text{H}_2\text{O}$, respectively.

Table 2. Calculated reaction energies for all hydrogenation elementary reactions on the Co (001) surface.

Reaction	E_{reaction} (eV)	E_{reaction} (eV) in Literature
$\text{CO} + \text{H} \rightarrow \text{COH}$	0.853	0.85(InZr ₃ (110)) [68], 1.04(PdCu ₃ (111)) [70]
$\text{CO} + \text{H} \rightarrow \text{HCO}$	0.574	0.80(Ni(110)) [64], 0.53(Cu ₃ Ag(211)) [69], 0.75(Cu(211)) [69]
$\text{COH} + \text{H} \rightarrow \text{cis-HCOH}$	0.858	-0.37 (PdCu ₃ (111)) [70], 0.14(Cu(111)) [71]
$\text{COH} + \text{H} \rightarrow \text{trans-HCOH}$	1.004	
$\text{HCO} + \text{H} \rightarrow \text{cis-HCOH}$	1.393	
$\text{HCO} + \text{H} \rightarrow \text{trans-HCOH}$	1.539	
$\text{cis-HCOH} + \text{H} \rightarrow \text{CH} + \text{H}_2\text{O}$	-0.773	
$\text{cis-HCOH} + \text{H} \rightarrow \text{CH}_2\text{OH}$	0.39	0.01(PdCu ₃ (111)) [70], 0.84(Cu(111)) [71]
$\text{trans-HCOH} + \text{H} \rightarrow \text{CH} + \text{H}_2\text{O}$	-1.283	
$\text{trans-HCOH} + \text{H} \rightarrow \text{CH}_2\text{OH}$	-0.12	0.01(PdCu ₃ (111)) [70], 0.77(Cu(111)) [71]
$\text{CH} + \text{H} \rightarrow \text{CH}_2$	0.019	0.35(InZr ₃ (110)) [68]
$\text{CH}_2 + \text{H} \rightarrow \text{CH}_3$	0.679	0.36(InZr ₃ (110)) [68]
$\text{CH}_3 + \text{H} \rightarrow \text{CH}_4$	0.491	
$\text{CH}_2\text{OH} + \text{H} \rightarrow \text{CH}_3\text{OH}$	0.089	0.49(Ni(110)) [64], 0.90(Cu(111)) [71]
$\text{CH} + \text{CH} \rightarrow \text{C}_2\text{H}_2$	1.511	

2.2. Analysis of the Kinetics

2.2.1. Transition States

The transition states of all the elementary reactions were identified and are shown in Figure 4. In order to gain further insight, the activation barriers for the elementary reactions in the CO hydrogenation process over the Co (001) surface were calculated and are listed in Table 3, where the energies were calculated via Equation (5).

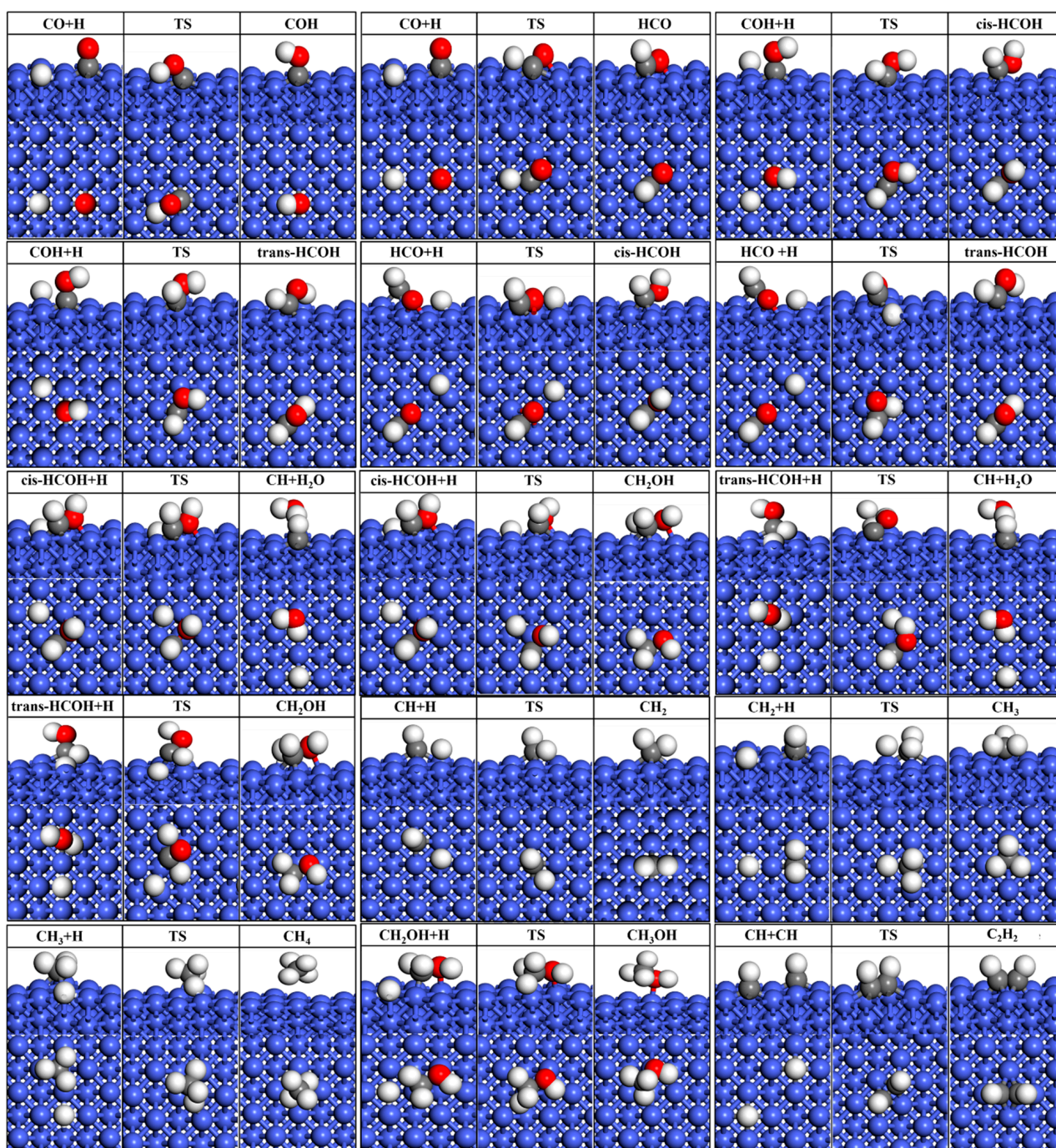


Figure 4. The reactions with their corresponding transition states on the Co (001) surface.

The energy barrier in the hydrogenation of CO is 1.804 eV for the production of COH, whereas it is 1.082 eV for the production of HCO, indicating that HCO is the preferred product from the first hydrogenation step. This finding is in good agreement with the literature, in which Zhu et al. [66] reported that the barrier for CO hydrogenation to COH on the Ni (111) surface is 1.97 eV, and Ashwell et al. [64] found a similar activation energy of 1.08 eV for the production of HCO over the Ni (110) surface. It is worth mentioning that among the reactions studied in this work, the reaction of $\text{CO} + \text{H} \rightarrow \text{COH}$ is the rate-determining step (RDS) on the Co (001) surface.

The energy barriers for COH hydrogenation to cis-HCOH and trans-HCOH are the same at 1.231 eV, which is comparable to the same reactions calculated by Amaya-Roncancio et al. [65] on

the Fe (100) surface at 1.38 eV. The hydrogenation reactions of HCO to reach the cis- and trans isomers of HCOH must overcome energy barriers of 1.746 and 1.727 eV, respectively.

Next, we consider the production of CH + H₂O and CH₂OH from the cis and trans conformers of HCOH. The barriers for the production of CH₂OH from the hydrogenation of either isomer are below 1 eV, at 0.662 and 0.131 eV for the cis-HCOH and trans-HCOH isomers, respectively, which is in good agreement with Qi et al. [72] who reported a barrier of 0.71 eV for cis-HCOH + H → CH₂OH on the Co (0001) surface. However, there is a large difference between the energy barriers to be overcome for the dissociation into CH + H₂O products from cis-HCOH or trans-HCOH in the presence of hydrogen. cis-HCOH dissociation produces CH + H₂O with a barrier of just 0.066 eV, but the production of CH + H₂O from trans-HCOH requires an activation energy of 1.581 eV. These results show that CH + H₂O and CH₂OH are more likely to be produced by the hydrogenation of cis-HCOH and trans-HCOH conformers, respectively, see Table 3.

The activation energy barrier for the synthesis of C₂H₂ from the reaction of CH + CH on the Co (001) surface is 1.556 eV, whereas the production of CH₃OH from the reaction of CH₂OH + H has a barrier of 0.725 eV. As discussed above, CH can be produced from either reaction of cis-HCOH + H → CH + H₂O or trans-HCOH + H → CH + H₂O, followed by further reaction with adsorbed hydrogens to produce CH₄ along three continuous reaction steps: CH + H, CH₂ + H, and CH₃ + H, with energy barriers of 0.065, 0.969, and 1.089 eV, respectively, see Table 3. These calculated energy barriers are in agreement with Zhu et al. [66], Cheng et al. [73], and Niu et al. [74], who reported activation energies of 0.69, 0.81, and 1.187 eV for this reaction on the Ni (111), Fe₅C₂ (100), and Pt (111) surfaces, respectively.

Table 3. Calculated activation energies (E_a) for all reactions on Co (001) surface.

Reaction	E _a (eV)	E _a (eV) In literature
CO + H → COH	1.804	1.55(Co(0001)) [72], 1.07(Fe(100)) [65], 1.97(Ni(111)) [66]
CO + H → HCO	1.082	1.08(Ni(110)) [64]
COH + H → cis – HCOH	1.231	1.38(Fe(100)) [65], 1.522(Pt(111)) [74]
COH + H → trans – HCOH	1.231	1.38(Fe(100)) [65], 1.522(Pt(111)) [74]
HCO + H → cis – HCOH	1.746	1.59(Co(0001)) [75]
HCO + H → trans – HCOH	1.727	1.59(Co(0001)) [75]
cis – HCOH + H → CH + H ₂ O	0.066	
cis – HCOH + H → CH ₂ OH	0.662	0.71(Co(0001)) [72], 0.43(Co(0001)) [75]
trans – HCOH + H → CH + H ₂ O	1.581	
trans – HCOH + H → CH ₂ OH	0.131	0.71(Co(0001)) [72], 0.43(Co(0001)) [75]
CH + CH → C ₂ H ₂	1.556	0.77(Ru(0001)) [31]
CH + H → CH ₂	0.065	0.69(Ni(111)) [66]
CH ₂ + H → CH ₃	0.969	0.81(Fe ₅ C ₂ (100)) [73], 1.360(Pt(111)) [74]
CH ₃ + H → CH ₄	1.089	1.187(Pt(111)) [74], 0.96(Fe ₅ C ₂ (100)) [73], 0.90(Ni(111)) [66]
CH ₂ OH + H → CH ₃ OH	0.725	1.04(Ni(110)) [64], 0.69(Ni(111)) [66], 0.82(Co(0001)) [75]

2.2.2. Reaction Pathways

The energies of the reaction routes to methanol, methane and acetylene production on the surface are shown in Figures 5–7, respectively. For each product, there are four pathways (Tables 4–6) through each of the routes of $\text{CO} \rightarrow \text{HCO} \rightarrow \text{cis-HCOH}$, $\text{CO} \rightarrow \text{HCO} \rightarrow \text{trans-HCOH}$, $\text{CO} \rightarrow \text{COH} \rightarrow \text{cis-HCOH}$, and $\text{CO} \rightarrow \text{COH} \rightarrow \text{trans-HCOH}$. Each product is reached through a main pathway with a favored reaction mechanism.

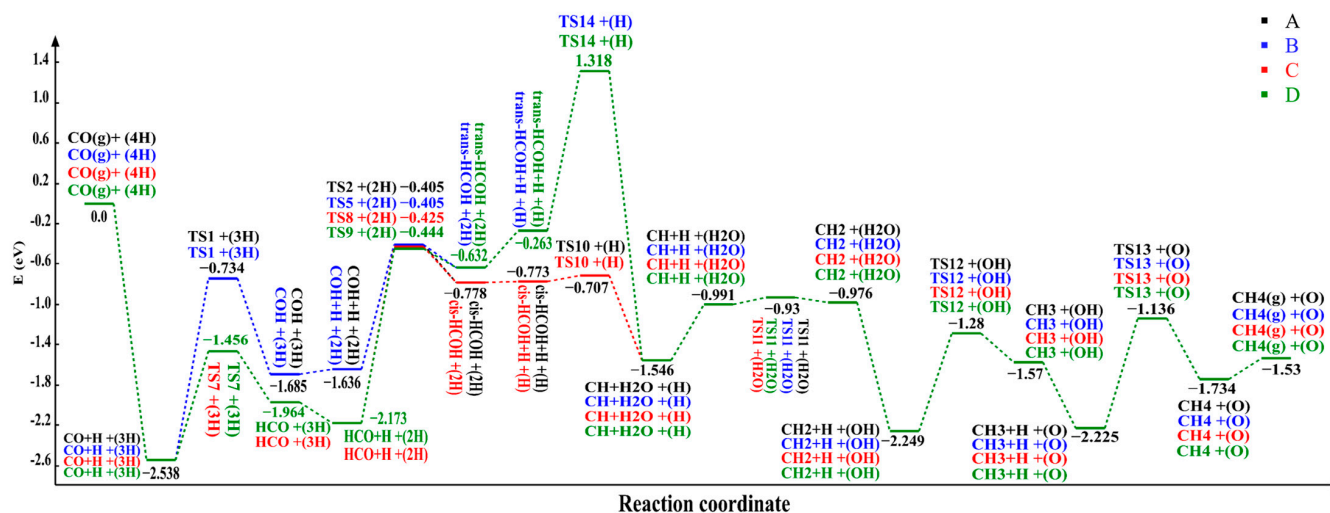


Figure 5. Four reaction pathways illustrating how the energies change in each path resulting in CH_4 production.

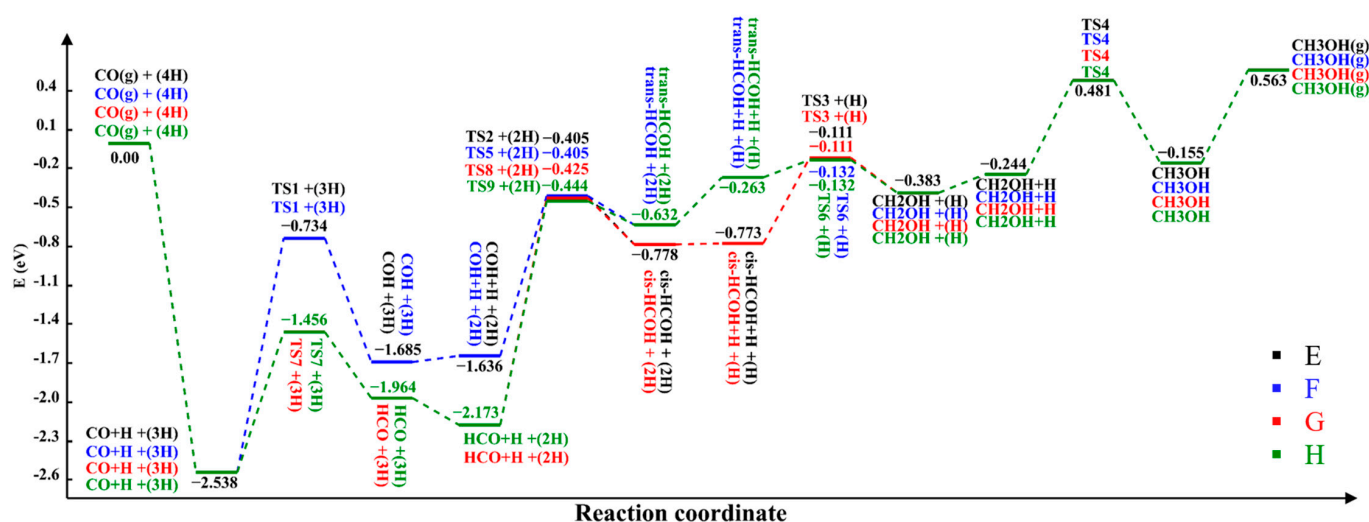


Figure 6. Four reaction pathways illustrating how the energies change in each path resulting in CH_3OH production.

CH_4 production can occur through CO hydrogenation via HCO and cis-HCOH intermediates. The reaction begins with the hydrogenation of CO. Then, according to the Figure 5 and Table 4, the pathways passing through HCO are the preferred route because the activation energy barrier for $\text{CO} + \text{H} \rightarrow \text{COH}$ is about 0.8 eV larger than for $\text{CO} + \text{H} \rightarrow \text{HCO}$. In the next step, HCO is hydrogenated to HCOH isomers ($\text{HCO} + \text{H} \rightarrow \text{cis-HCOH}$ and $\text{HCO} + \text{H} \rightarrow \text{trans-HCOH}$). Although these two reactions are kinetically the same, thermodynamically, cis-HCOH is the preferred intermediate, resulting in the reaction sequences $\text{CH} + \text{H} \rightarrow \text{CH}_2$, $\text{CH}_2 + \text{H} \rightarrow \text{CH}_3$ and $\text{CH}_3 + \text{H} \rightarrow \text{CH}_4$ being the most favorable route for CH_4 production (Figure 5). This pathway is completely exothermic, with an overall reaction energy of -1.53 eV, and the hydrogenation of $\text{cis-HCOH} + \text{H} \rightarrow \text{CH} + \text{H}_2\text{O}$ is

the most favorable reaction in this pathway, with an energy of -0.773 eV. In contrast, the least favourable reaction is $\text{HCO} + \text{H} \rightarrow \text{cis-HCOH}$, which requires 1.393 eV of energy. Kinetically, the hydrogenation of $\text{CH} + \text{H} \rightarrow \text{CH}_2$ is the optimum reaction in this pathway, with an energy barrier of only 0.065 eV.

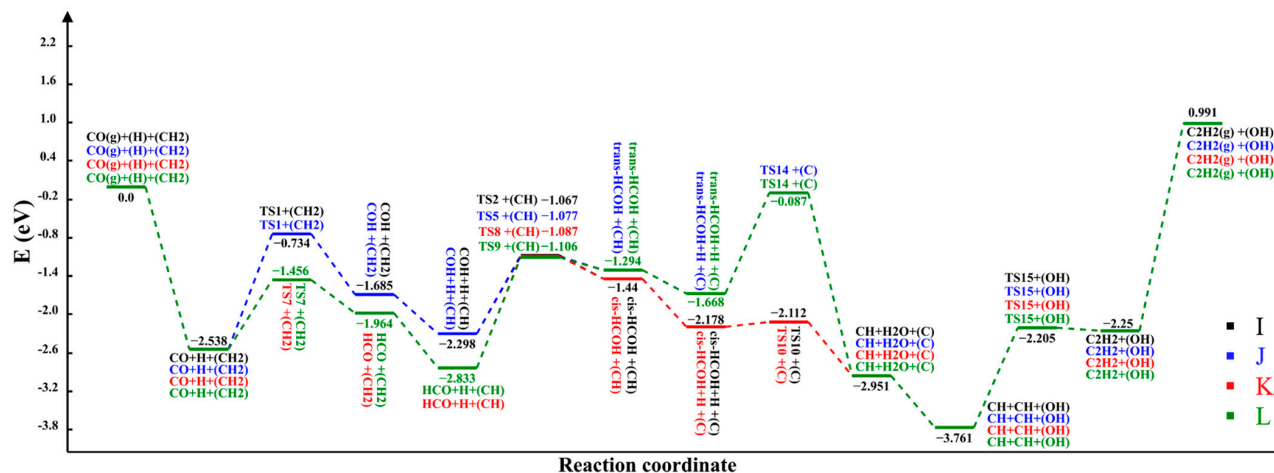


Figure 7. Four reaction pathways illustrating how the energies change in each path resulting in C_2H_2 production.

Table 4. Four paths resulting in CH_4 . Energies are related to the CO in the gas phase plus the energy of four hydrogen atoms on the surface. The symbols in parentheses are the atoms added along the paths to balance the number of atoms during reaction profile.

Path A		Path B		Path C		Path D	
State	E (eV)						
$\text{CO}(\text{g})+(4\text{H})$	0.00	$\text{CO}(\text{g})+(4\text{H})$	0.00	$\text{CO}(\text{g})+(4\text{H})$	0.00	$\text{CO}(\text{g})+(4\text{H})$	0.00
$\text{CO}+\text{H}+(3\text{H})$	-2.538	$\text{CO}+\text{H}+(3\text{H})$	-2.538	$\text{CO}+\text{H}+(3\text{H})$	-2.538	$\text{CO}+\text{H}+(3\text{H})$	-2.538
$\text{TS1}+(3\text{H})$	-0.734	$\text{TS1}+(3\text{H})$	-0.734	$\text{TS7}+(3\text{H})$	-1.456	$\text{TS7}+(3\text{H})$	-1.456
$\text{COH}+(3\text{H})$	-1.685	$\text{COH}+(3\text{H})$	-1.685	$\text{HCO}+(3\text{H})$	-1.964	$\text{HCO}+(3\text{H})$	-1.964
$\text{COH}+\text{H}+(2\text{H})$	-1.636	$\text{COH}+\text{H}+(2\text{H})$	-1.636	$\text{HCO}+\text{H}+(2\text{H})$	-2.173	$\text{HCO}+\text{H}+(2\text{H})$	-2.173
$\text{TS2}+(2\text{H})$	-0.405	$\text{TS5}+(2\text{H})$	-0.405	$\text{TS8}+(2\text{H})$	-0.425	$\text{TS9}+(2\text{H})$	-0.444
$\text{cis-HCOH}+(2\text{H})$	-0.778	$\text{trans-HCOH}+(2\text{H})$	-0.632	$\text{cis-HCOH}+(2\text{H})$	-0.778	$\text{trans-HCOH}+(2\text{H})$	-0.632
$\text{cis-HCOH}+\text{H}+(\text{H})$	-0.773	$\text{trans-HCOH}+\text{H}+(\text{H})$	-0.263	$\text{cis-HCOH}+\text{H}+(\text{H})$	-0.773	$\text{trans-HCOH}+\text{H}+(\text{H})$	-0.263
$\text{TS10}+(\text{H})$	-0.707	$\text{TS14}+(\text{H})$	1.318	$\text{TS10}+(\text{H})$	-0.707	$\text{TS14}+(\text{H})$	1.318
$\text{CH}+\text{H}_2\text{O}+(\text{H})$	-1.546	$\text{CH}+\text{H}_2\text{O}+(\text{H})$	-1.546	$\text{CH}+\text{H}_2\text{O}+(\text{H})$	-1.546	$\text{CH}+\text{H}_2\text{O}+(\text{H})$	-1.546
$\text{CH}+\text{H}+(\text{H}_2\text{O})$	-0.991	$\text{CH}+\text{H}+(\text{H}_2\text{O})$	-0.991	$\text{CH}+\text{H}+(\text{H}_2\text{O})$	-0.991	$\text{CH}+\text{H}+(\text{H}_2\text{O})$	-0.991
$\text{TS11}+(\text{H}_2\text{O})$	-0.93	$\text{TS11}+(\text{H}_2\text{O})$	-0.93	$\text{TS11}+(\text{H}_2\text{O})$	-0.93	$\text{TS11}+(\text{H}_2\text{O})$	-0.93
$\text{CH}_2+(\text{H}_2\text{O})$	-0.976	$\text{CH}_2+(\text{H}_2\text{O})$	-0.976	$\text{CH}_2+(\text{H}_2\text{O})$	-0.976	$\text{CH}_2+(\text{H}_2\text{O})$	-0.976
$\text{CH}_2+\text{H}+(\text{OH})$	-2.249	$\text{CH}_2+\text{H}+(\text{OH})$	-2.249	$\text{CH}_2+\text{H}+(\text{OH})$	-2.249	$\text{CH}_2+\text{H}+(\text{OH})$	-2.249
$\text{TS12}+(\text{OH})$	-1.28	$\text{TS12}+(\text{OH})$	-1.28	$\text{TS12}+(\text{OH})$	-1.28	$\text{TS12}+(\text{OH})$	-1.28
$\text{CH}_3+(\text{OH})$	-1.57	$\text{CH}_3+(\text{OH})$	-1.57	$\text{CH}_3+(\text{OH})$	-1.57	$\text{CH}_3+(\text{OH})$	-1.57
$\text{CH}_3+\text{H}+(\text{O})$	-2.225	$\text{CH}_3+\text{H}+(\text{O})$	-2.225	$\text{CH}_3+\text{H}+(\text{O})$	-2.225	$\text{CH}_3+\text{H}+(\text{O})$	-2.225
$\text{TS13}+(\text{O})$	-1.136	$\text{TS13}+(\text{O})$	-1.136	$\text{TS13}+(\text{O})$	-1.136	$\text{TS13}+(\text{O})$	-1.136
$\text{CH}_4+(\text{O})$	-1.734	$\text{CH}_4+(\text{O})$	-1.734	$\text{CH}_4+(\text{O})$	-1.734	$\text{CH}_4+(\text{O})$	-1.734
$\text{CH}_4(\text{g})+(\text{O})$	-1.53	$\text{CH}_4(\text{g})+(\text{O})$	-1.53	$\text{CH}_4(\text{g})+(\text{O})$	-1.53	$\text{CH}_4(\text{g})+(\text{O})$	-1.53

The kinetic and thermodynamic outcomes for the byproducts indicate that the favored pathways resulting in CH_3OH and C_2H_2 (presented in Tables 5 and 6) have the same intermediates in the first two steps, beginning with $\text{CO} + \text{H} \rightarrow \text{HCO}$ and then passing through $\text{HCO} + \text{H} \rightarrow \text{cis-HCOH}$. In the production of CH_3OH , the $\text{cis-HCOH} + \text{H} \rightarrow \text{CH}_2\text{OH}$ reac-

tion costs 0.39 eV, with a barrier of 0.662 eV, followed by the reaction of $\text{CH}_2\text{OH} + \text{H} \rightarrow \text{CH}_3\text{OH}$, which requires 0.089 eV and must overcome a barrier of 0.725 eV to proceed. Cis-HCOH is hydrogenated to C_2H_2 by the reaction sequences of $\text{cis-HCOH} + \text{H} \rightarrow \text{CH} + \text{H}_2\text{O}$ and $\text{CH} + \text{CH} \rightarrow \text{C}_2\text{H}_2$, with reaction energies of -0.773 and 1.511 eV and energy barriers of 0.066 and 1.556 eV (Figures 6 and 7). The optimum pathways for the production of CH_3OH and C_2H_2 are entirely endothermic, with overall reaction energies of 0.563, and 0.991 eV, respectively. The most favorable reaction in the production of C_2H_2 is cis-HCOH to $\text{CH} + \text{H}_2\text{O}$, with an energy of -0.773 eV, and in the CH_3OH formation, it is the hydrogenation of cis-HCOH to CH_2OH , with an energy of 0.39 eV.

Table 5. Four paths resulting in CH_3OH . Energies are related to the CO in the gas phase plus the energy of four hydrogen atoms on the surface. The symbols in parentheses are the atoms added along the paths to balance the number of atoms during reaction profile.

Path E		Path F		Path G		Path H	
State	E (eV)						
CO(g)+(4H)	0.00	CO(g)+(4H)	0.00	CO(g)+(4H)	0.00	CO(g)+(4H)	0.00
CO+H+(3H)	-2.538	CO+H+(3H)	-2.538	CO+H+(3H)	-2.538	CO+H+(3H)	-2.538
TS1+(3H)	-0.734	TS1+(3H)	-0.734	TS7+(3H)	-1.456	TS7+(3H)	-1.456
COH+(3H)	-1.685	COH+(3H)	-1.685	HCO+(3H)	-1.964	HCO+(3H)	-1.964
COH+H+(2H)	-1.636	COH+H+(2H)	-1.636	HCO+H+(2H)	-2.173	HCO+H+(2H)	-2.173
TS2+(2H)	-0.405	TS5+(2H)	-0.405	TS8+(2H)	-0.425	TS9+(2H)	-0.444
cis-HCOH+(2H)	-0.778	trans-HCOH+(2H)	-0.632	cis-HCOH+(2H)	-0.778	trans-HCOH+(2H)	-0.632
cis-HCOH+H+(H)	-0.773	trans-HCOH+H+(H)	-0.263	cis-HCOH+H+(H)	-0.773	trans-HCOH+H+(H)	-0.263
TS3+(H)	-0.111	TS6+(H)	-0.132	TS3+(H)	-0.111	TS6+(H)	-0.132
CH ₂ OH+(H)	-0.383						
CH ₂ OH+H	-0.244						
TS4	0.481	TS4	0.481	TS4	0.481	TS4	0.481
CH ₃ OH	-0.155						
CH ₃ OH (g)	0.563						

Table 6. Four paths resulting in C_2H_2 . Energies are related to the CO in the gas phase plus the energy of one hydrogen atom and one CH_2 on the surface. The symbols in parentheses are the atoms added along the paths to balance the number of atoms during reaction profile.

Path I		Path J		Path K		Path L	
state	E (eV)						
CO(g)+(H)+(CH ₂)	0.00						
CO+H+(CH ₂)	-2.538						
TS1+(CH ₂)	-0.734	TS1+(CH ₂)	-0.734	TS7+(CH ₂)	-1.456	TS7+(CH ₂)	-1.456
COH+(CH ₂)	-1.685	COH+(CH ₂)	-1.685	HCO+(CH ₂)	-1.964	HCO+(CH ₂)	-1.964
COH+H+(CH)	-2.298	COH+H+(CH)	-2.298	HCO+H+(CH)	-2.833	HCO+H+(CH)	-2.833
TS2+(CH)	-1.067	TS5+(CH)	-1.077	TS8+(CH)	-1.087	TS9+(CH)	-1.106
cis-HCOH+(CH)	-1.44	trans-HCOH+(CH)	-1.294	cis-HCOH+(CH)	-1.44	trans-HCOH+(CH)	-1.294
cis-HCOH+H+(C)	-2.178	trans-HCOH+H+(C)	-1.668	cis-HCOH+H+(C)	-2.178	trans-HCOH+H+(C)	-1.668
TS10+(C)	-2.112	TS14+(C)	-0.087	TS10+(C)	-2.112	TS14+(C)	-0.087
CH+H ₂ O+(C)	-2.951						
CH+CH+(OH)	-3.761	CH+CH+(OH)	-3.761	CH+CH+(OH)	-3.761	CH+CH+(OH)	-3.761
TS15+(OH)	-2.205	TS15+(OH)	-2.205	TS15+(OH)	-2.205	TS15+(OH)	2.205
C ₂ H ₂ +(OH)	-2.25						
C ₂ H ₂ (g)+(OH)	0.991						

Based on kinetic and thermodynamic considerations, path C appears the most likely pathway, shown in Figure 8, leading to CH_4 as the product. The selectivity of this pathway

3.2. Model

Metallic cobalt can crystallize in two different crystal structures: a hexagonal closed-packed (hcp) structure and a face-centered cubic (fcc) structure [91–94]. These two phases possess similar energetic stabilities; hence, small temperature or pressure variations give rise to changes in the crystal phase. This similar stability also renders theoretical predictions difficult for either the bulk or nanoparticles [91]. The fcc bulk crystal structure of cobalt was selected in this study, and we investigate the Fischer–Tropsch synthesis mechanism on its (001) plane. Figure 9 shows the primitive cell in the fcc crystal system with a lattice parameter of 3.42 Å, which was downloaded from MaterialsProject [95] with the name “Co_mp-102”. According to the literature, the Fischer–Tropsch synthesis of carbon monoxide hydrogenation over hcp cobalt goes through the direct dissociation of the C–O bond, while H-assisted dissociation of the C–O is the preferred mechanism over fcc cobalt [96]. In this study of the fcc Co (001) plane, we investigated H-assisted CO dissociation, followed by further hydrogenation reactions.

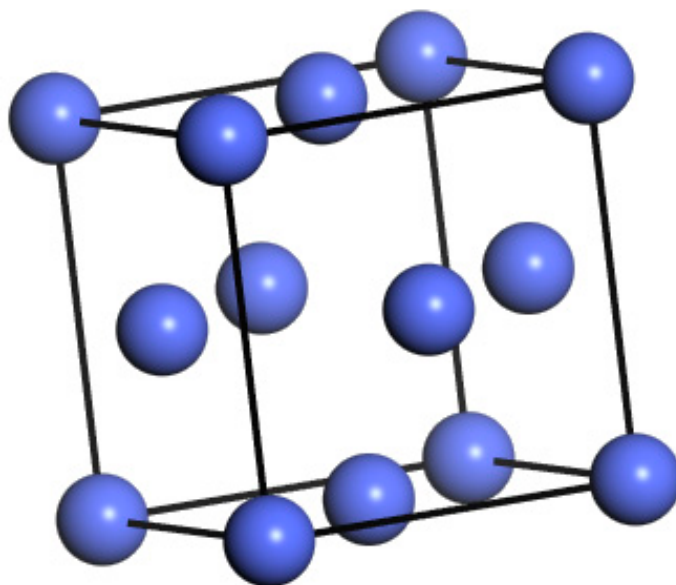


Figure 9. Bulk structure of fcc cobalt.

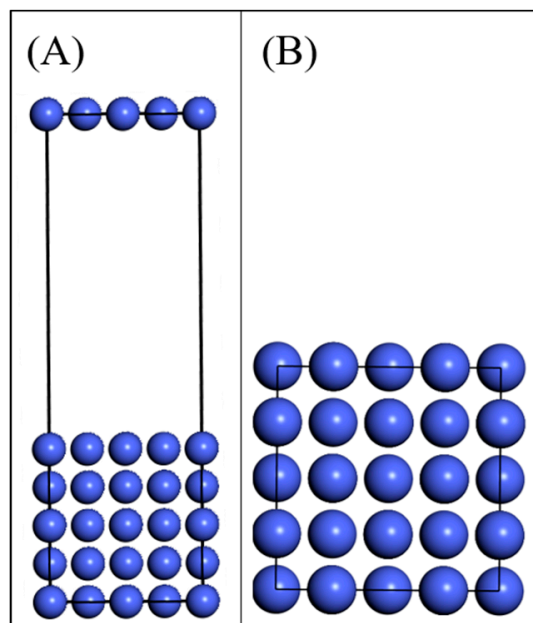
The optimized bulk structure was cleaved to obtain the (001) surface using Materials studio [59]. The supercell was expanded to $3 \times 3 \times 1$ with dimensions of $6.841 \times 6.841 \times 21.841$ Å to ensure we had enough space for the adsorption of the molecules on the surface. Slabs with different thicknesses of three to eight layers were created, and their surface energies, E_{surf} , were calculated using Equation (1):

$$E_{surf} = \frac{[E_{tot}(slab) - nE_{tot}(bulk)]}{2A} \quad (1)$$

where A is the cross-sectional area of the surface slab, $E_{tot}(bulk)$ refers to the energy of a unit cell of the bulk metal per atom, $E_{tot}(slab)$ is the total energy of the slab, and n denotes the number of atoms in the slab. The surface energy was calculated for all slabs with different thicknesses. According to Table 7, the five-layer slab of cobalt atoms, shown in Figure 10, converged sufficiently and offered the optimum balance between a sufficient number of layers to enable surface relaxation and speed of calculation. The calculated surface energy for the Co (001) surface (Table 7) agrees well with values in the literature (3.40 J/m^2) [97].

Table 7. Calculated surface energies in (J/m^2) for Co (001) slabs with different thicknesses.

Number of Layers	$E_{surf}(\text{J}/\text{m}^2)$
3	3.590
4	3.647
5	3.639
6	3.626
7	3.639
8	3.632

**Figure 10.** Co (001) slab from (A) side and (B) top views.

To determine the optimum number of relaxed layers in the slab, we examined slabs with different numbers of layers, from one to four, that were allowed to relax unrestrainedly, while the rest of the layers were fixed in their bulk positions. The surface energy was then calculated as:

$$\gamma_r = \frac{E_{slab,relaxed} - nE_{bulk}}{A} - \frac{E_{slab,unrelaxed} - nE_{bulk}}{2A} \quad (2)$$

where $E_{slab,relaxed}$ is the energy of the slab with a number of relaxed and fixed layers, whereas $E_{slab,unrelaxed}$ is the energy of the fixed-layer slab. Table 8 shows the relaxed surface energies with respect to the number of fixed layers for different slabs. According to the results, the surface energy converged for the slab with two fixed and three relaxed layers, i.e., apart from the constrained bottom two layers of the slab, all atoms were allowed to relax explicitly upon optimization. The vacuum space was introduced on top of the slab to avoid interactions between the slab images in the Z direction of the cell.

Table 8. Calculated relaxed surface energies in (J/m^2) for Co (001) slabs with the different number of fixed layers.

Number of the Fixed Layers	$\gamma_r(\text{J}/\text{m}^2)$
1	4.492
2	4.495
3	4.4955
4	4.4955

The adsorption energy of the adsorbates (E_{ads}) can be calculated using Equation (3):

$$E_{ads} = E_{slab+mol} - (E_{mol} + E_{slab}) \quad (3)$$

where $E_{slab+mol}$ is the energy of the relaxed molecule on the relaxed surface, E_{mol} is the lowest energy of the optimized molecule in a vacuum, and E_{slab} is the total energy of the relaxed surface.

The reaction ($E_{reaction}$) and activation ($E_{activation}$) energies of each reaction can be calculated using Equations (4) and (5), respectively:

$$E_{reaction} = E_{product} - E_{reactant} \quad (4)$$

$$E_{activation} = E_{transitionstate} - E_{reactant} \quad (5)$$

4. Conclusions

Calculations based on the density functional theory were employed to unravel the conversion of a mixture of hydrogen and carbon monoxide into hydrocarbons over the Co (001) surface, which has provided valuable insights into the mechanism of CO hydrogenation over the Co (001) surface in Fischer–Tropsch synthesis. We also identified several key intermediates and transition states involved in the elementary reactions, which can be used to guide the design of more efficient and selective Co-based catalysts for industrial applications.

The calculated adsorption energies of different intermediates on the Co (001) surface show that the CH_4 and CH_3OH products adsorbed with energies of -0.204 and -0.718 eV at hollow and top positions, respectively, whereas C_2H_2 adsorbed with an energy of -3.241 eV in a hollow site, confirming that CH_4 and CH_3OH are more easily desorbed from the Co (001) surface than C_2H_2 .

The formation of methane, methanol, and acetylene was found to proceed via the hydrogenation of the carbon end of CO to HCO, followed by hydrogenation to cis-HCOH, and via the CH_2OH intermediate to methanol, which can then be further hydrogenated to methane and acetylene through CH intermediates. The preferred mechanism resulting in CH_4 as the favored product begins with the reactions $\text{CO} + \text{H} \rightarrow \text{HCO}$ and $\text{HCO} + \text{H} \rightarrow \text{cis-HCOH}$, followed by $\text{cis-HCOH} + \text{H} \rightarrow \text{CH} + \text{H}_2\text{O}$. Next, CH is hydrogenated to CH_4 along the reactions $\text{CH} + \text{H} \rightarrow \text{CH}_2$, $\text{CH}_2 + \text{H} \rightarrow \text{CH}_3$ and $\text{CH}_3 + \text{H} \rightarrow \text{CH}_4$. For the other products, the preferred mechanisms are the same until cis-HCOH formation, whence CH_3OH is produced through the CH_2OH intermediate, and C_2H_2 results from the reaction between two CHs that were produced through the hydrogenation of cis-HCOH. The optimum pathways for CH_4 , CH_3OH , and C_2H_2 production proceed with overall energies of -1.53 , 0.563 , and 0.991 eV, respectively. The reaction $\text{HCO} + \text{H} \rightarrow \text{cis-HCOH}$, with an activation energy of 1.746 eV, has the highest energy barrier in the selected pathways.

We consider that this study has provided important understanding of the catalytic processes involved in the hydrogenation of carbon monoxide over the Co (001) surface with implications for Fischer–Tropsch synthesis.

Supplementary Materials: The following supporting information can be downloaded at: <https://www.mdpi.com/article/10.3390/catal13050837/s1>, Figure S1: Side views of the lowest-energy adsorption configurations of each intermediate on Co (001) surface. The bond lengths are shown in Å. The gray, white, red, and blue balls represent carbon, hydrogen, oxygen, and cobalt atoms, respectively; Table S1: The structural details of the preferred adsorption geometries for all intermediates on the Co (001) surface.

Author Contributions: Conceptualization, S.S.T. and N.H.d.L.; methodology, S.S.T.; software, S.S.T. and M.T.; validation, S.S.T. and N.H.d.L.; formal analysis, S.S.T. and N.H.d.L.; investigation, M.T.; resources, N.H.d.L.; data curation, M.T.; writing—original draft preparation, M.T.; writing—review and editing, S.S.T. and N.H.d.L.; visualization, M.T.; supervision, S.S.T. and N.H.d.L.; project administration, S.S.T.; funding acquisition, S.S.T. and N.H.d.L. All authors have read and agreed to the published version of the manuscript.

Funding: This research received no external funding.

Data Availability Statement: The data presented in this study are available on request from the corresponding authors.

Acknowledgments: S.S.T. appreciates the Research Affairs Division of the Amirkabir University of Technology (AUT), Tehran, Iran, for their financial support. This work used the computational facilities of the Advanced Research Computing at Cardiff (ARCCA) Division, Cardiff University, and HPC Wales, via our membership in the UK's HEC Materials Chemistry Consortium, which is funded by EPSRC (EP/R029431). This work also used the ARCHER2 UK National Supercomputing Service (<http://archer2.ac.uk>), accessed on 20 April 2023.

Conflicts of Interest: The authors declare no conflict of interest.

References

1. Byard, R.W. Carbon Monoxide – the Silent Killer. *Forensic Sci. Med. Pathol.* **2019**, *15*, 1–2. [[CrossRef](#)]
2. Can, G.; Sayılı, U.; Aksu Sayman, Ö.; Kuyumcu, Ö.F.; Yılmaz, D.; Esen, E.; Yurtseven, E.; Erginöz, E. Mapping of Carbon Monoxide Related Death Risk in Turkey: A Ten-Year Analysis Based on News Agency Records. *BMC Public Health* **2019**, *19*, 9. [[CrossRef](#)]
3. Kinoshita, H.; Türkan, H.; Vucinic, S.; Naqvi, S.; Bedair, R.; Rezaee, R.; Tsatsakis, A. Carbon Monoxide Poisoning. *Toxicol. Rep.* **2020**, *7*, 169–173. [[CrossRef](#)]
4. Fujimori, S.; Inoue, S. Carbon Monoxide in Main-Group Chemistry. *J. Am. Chem. Soc.* **2022**, *144*, 2034–2050. [[CrossRef](#)]
5. Elenhorn, M.J. *Medical Toxicology Diagnosis and Treatment of Human Poisoning*; Williams & Wilkins: Baltimore, MD, USA, 1997.
6. Baselt, R.C.; Cravey, R.H. *Disposition of Toxic Drugs and Chemicals in Man*; Biomedical publications: Davis, CA, USA, 1982; Volume 33.
7. Jager, B.; Espinoza, R. Advances in Low Temperature Fischer-Tropsch Synthesis. *Catal. Today* **1995**, *23*, 17–28. [[CrossRef](#)]
8. Biloen, P. On the Activity of Fischer-Tropsch and Methanation Catalysts: A Study Utilizing Isotopic Transients. *J. Catal.* **1983**, *81*, 450–463. [[CrossRef](#)]
9. Dry, M.E. Practical and Theoretical Aspects of the Catalytic Fischer-Tropsch Process. *Appl. Catal. A Gen.* **1996**, *138*, 319–344. [[CrossRef](#)]
10. Geerlings, J.J.C.; Wilson, J.H.; Kramer, G.J.; Kuipers, H.P.C.E.; Hoek, A.; Huisman, H.M. Fischer-Tropsch Technology — from Active Site to Commercial Process. *Appl. Catal. A Gen.* **1999**, *186*, 27–40. [[CrossRef](#)]
11. Dry, M.E. The Fischer-Tropsch Process: 1950–2000. *Catal. Today* **2002**, *71*, 227–241. [[CrossRef](#)]
12. Schweicher, J.; Bundhoo, A.; Frennet, A.; Kruse, N.; Daly, H.; Meunier, F.C. DRIFTS/MS Studies during Chemical Transients and SSITKA of the CO/H₂ Reaction over Co-MgO Catalysts. *J. Phys. Chem. C* **2010**, *114*, 2248–2255. [[CrossRef](#)]
13. Roldan, A.; De Leeuw, N.H. Selective Hydrogenation of CO on Fe₃S₄ {111}: A Computational Study. *Faraday Discuss.* **2017**, *197*, 325–336. [[CrossRef](#)]
14. Cheng, J.; Hu, P.; Ellis, P.; French, S.; Kelly, G.; Lok, C. A DFT Study of the Chain Growth Probability in Fischer-Tropsch Synthesis. *J. Catal.* **2008**, *257*, 221–228. [[CrossRef](#)]
15. Liu, J.; Chen, Y.; Wei, J.; Duyar, M.S.; Ordonsky, V.V.; Khodakov, A.Y. Chem Soc Rev Chemical Society Reviews Carbon-Based Catalysts for Fischer-Tropsch Synthesis. *Chem. Soc. Rev.* **2021**, *50*, 2337. [[CrossRef](#)]
16. Zhang, Z.; Chen, X.; Kang, J.; Yu, Z.; Tian, J.; Gong, Z.; Jia, A.; You, R.; Qian, K.; He, S.; et al. The Active Sites of Cu-ZnO Catalysts for Water Gas Shift and CO Hydrogenation Reactions. *Nat. Commun.* **2021**, *12*, 4331. [[CrossRef](#)]
17. Ye, A.; Li, Z.; Ding, J.; Xiong, W.; Huang, W. Synergistic Catalysis of Al and Zn Sites of Spinel ZnAl₂O₄ Catalyst for CO Hydrogenation to Methanol and Dimethyl Ether. *ACS Catal.* **2021**, *11*, 10014–10019. [[CrossRef](#)]
18. Fang, W.; Wang, C.; Liu, Z.; Wang, L.; Liu, L.; Li, H.; Xu, S.; Zheng, A.; Qin, X.; Liu, L.; et al. Physical Mixing of a Catalyst and a Hydrophobic Polymer Promotes CO Hydrogenation through Dehydration. *Science* **2022**, *377*, 406–410. [[CrossRef](#)] [[PubMed](#)]
19. Li, Z.; Zhang, X.; Liu, J.; Shi, R.; Waterhouse, G.I.N.; Wen, X.; Zhang, T. Titania-Supported Ni₂P/Ni Catalysts for Selective Solar-Driven CO Hydrogenation. *Adv. Mater.* **2021**, *33*, 2103248. [[CrossRef](#)]
20. Zhang, C.; Li, S.; Zhong, L.; Sun, Y. Theoretical Insights into Morphologies of Alkali-Promoted Cobalt Carbide Catalysts for Fischer-Tropsch Synthesis. *J. Phys. Chem. C* **2021**, *125*, 6061–6072. [[CrossRef](#)]
21. Chan, A.Y.; Perry, I.B.; Bissonnette, N.B.; Buksh, B.F.; Edwards, G.A.; Frye, L.I.; Garry, O.L.; Lavagnino, M.N.; Li, B.X.; Liang, Y.; et al. Metallaphotoredox: The Merger of Photoredox and Transition Metal Catalysis. *Chem. Rev.* **2022**, *122*, 1485–1542. [[CrossRef](#)] [[PubMed](#)]
22. Cheng, J.; Song, T.; Hu, P.; Lok, C.M.; Ellis, P.; French, S. A Density Functional Theory Study of the α -Olefin Selectivity in Fischer-Tropsch Synthesis. *J. Catal.* **2008**, *255*, 20–28. [[CrossRef](#)]
23. Cheng, J.; Gong, X.Q.; Hu, P.; Lok, C.M.; Ellis, P.; French, S. A Quantitative Determination of Reaction Mechanisms from Density Functional Theory Calculations: Fischer-Tropsch Synthesis on Flat and Stepped Cobalt Surfaces. *J. Catal.* **2008**, *254*, 285–295. [[CrossRef](#)]
24. Zijlstra, B.; Broos, R.J.P.; Chen, W.; Pilot, I.A.W.; Hensen, E.J.M. First-Principles Based Microkinetic Modeling of Transient Kinetics of CO Hydrogenation on Cobalt Catalysts. *Catal. Today* **2020**, *342*, 131–141. [[CrossRef](#)]

25. Studt, F.; Abild-Pedersen, F.; Wu, Q.; Jensen, A.D.; Temel, B.; Grunwaldt, J.D.; Norskov, J.K. CO Hydrogenation to Methanol on Cu-Ni Catalysts: Theory and Experiment. *J. Catal.* **2012**, *293*, 51–60. [[CrossRef](#)]
26. Loveless, B.T.; Buda, C.; Neurock, M.; Iglesia, E. CO Chemisorption and Dissociation at High Coverages during CO Hydrogenation on Ru Catalysts. *J. Am. Chem. Soc.* **2013**, *135*, 6107–6121. [[CrossRef](#)] [[PubMed](#)]
27. Zhuo, M.; Fei Tan, K.; Borgna, A.; Saeys, M. Density Functional Theory Study of the CO Insertion Mechanism for Fischer–Tropsch Synthesis over Co Catalysts. *J. Phys. Chem. C* **2009**, *113*, 8357–8365. [[CrossRef](#)]
28. Lin, S.; Ma, J.; Ye, X.; Xie, D.; Guo, H. CO Hydrogenation on Pd(111): Competition between Fischer-Tropsch and Oxygenate Synthesis Pathways. *J. Phys. Chem. C* **2013**, *117*, 14667–14674. [[CrossRef](#)]
29. Zhang, M.; Wu, Y.; Dou, M.; Yu, Y. A DFT Study of Methanol Synthesis from CO₂ Hydrogenation on the Pd(111) Surface. *Catal. Lett.* **2018**, *148*, 2935–2944. [[CrossRef](#)]
30. Ge, Q.; Neurock, M. Adsorption and Activation of CO over Flat and Stepped Co Surfaces: A First Principles Analysis. *J. Phys. Chem. B* **2006**, *110*, 15368–15380. [[CrossRef](#)]
31. Zhang, S.T.; Yan, H.; Wei, M.; Evans, D.G.; Duan, X. Hydrogenation Mechanism of Carbon Dioxide and Carbon Monoxide on Ru(0001) Surface: A Density Functional Theory Study. *RSC Adv.* **2014**, *4*, 30241–30249. [[CrossRef](#)]
32. Dragutan, V.; Dragutan, I.; Xiong, G.; You, L.; Sun, Y.; Ding, F. Recent Developments on Carbon-Carbon Cross-Coupling Reactions Using Rare-Earth Metals-Derived Coordination Polymers as Efficient and Selective Pd Catalytic Systems. *Resour. Chem. Mater.* **2022**, *1*, 325–338. [[CrossRef](#)]
33. Molnár, Á. Efficient, Selective, and Recyclable Palladium Catalysts in Carbon–Carbon Coupling Reactions. *Chem. Rev.* **2011**, *111*, 2251–2320. [[CrossRef](#)] [[PubMed](#)]
34. Takeda, Y.; Ikeda, Y.; Kuroda, A.; Tanaka, S.; Minakata, S. Pd/NHC-Catalyzed Enantiospecific and Regioselective Suzuki–Miyaura Arylation of 2-Arylaziridines: Synthesis of Enantioenriched 2-Arylphenethylamine Derivatives. *J. Am. Chem. Soc.* **2014**, *136*, 8544–8547. [[CrossRef](#)] [[PubMed](#)]
35. Masson-Makdissi, J.; Vandavasi, J.K.; Newman, S.G. Switchable Selectivity in the Pd-Catalyzed Alkylative Cross-Coupling of Esters. *Org. Lett.* **2018**, *20*, 4094–4098. [[CrossRef](#)] [[PubMed](#)]
36. Molander, G.A.; Trice, S.L.J.; Kennedy, S.M. Scope of the Two-Step, One-Pot Palladium-Catalyzed Borylation/Suzuki Cross-Coupling Reaction Utilizing Bis-Boronic Acid. *J. Org. Chem.* **2012**, *77*, 8678–8688. [[CrossRef](#)]
37. Hoshi, T.; Honma, T.; Mori, A.; Konishi, M.; Sato, T.; Hagiwara, H.; Suzuki, T. An Active, General, and Long-Lived Palladium Catalyst for Cross-Couplings of Deactivated (Hetero) Aryl Chlorides and Bromides with Arylboronic Acids. *J. Org. Chem.* **2013**, *78*, 11513–11524. [[CrossRef](#)]
38. Li, L.; Zhao, S.; Joshi-Pangu, A.; Diane, M.; Biscoe, M.R. Stereospecific Pd-Catalyzed Cross-Coupling Reactions of Secondary Alkylboron Nucleophiles and Aryl Chlorides. *J. Am. Chem. Soc.* **2014**, *136*, 14027–14030. [[CrossRef](#)] [[PubMed](#)]
39. Martínez, R.; Pastor, I.M.; Yus, M. Biscarboxy-Functionalized Imidazole and Palladium as Highly Active Catalytic System in Protic Solvents: Methanol and Water. *Synthesis* **2014**, *46*, 2965–2975. [[CrossRef](#)]
40. Tu, T.; Sun, Z.; Fang, W.; Xu, M.; Zhou, Y. Robust Acenaphthoimidazolylidene Palladium Complexes: Highly Efficient Catalysts for Suzuki–Miyaura Couplings with Sterically Hindered Substrates. *Org. Lett.* **2012**, *14*, 4250–4253. [[CrossRef](#)]
41. Tang, J.-S.; Tian, M.; Sheng, W.-B.; Guo, C.-C. Efficient Palladium-Catalyzed Cross-Coupling Reaction of Alkynyl Halides with Organoboronic Acids under Aerobic Conditions. *Synthesis* **2012**, *44*, 541–546. [[CrossRef](#)]
42. Ben Halima, T.; Zhang, W.; Yalaoui, I.; Hong, X.; Yang, Y.-F.; Houk, K.N.; Newman, S.G. Palladium-Catalyzed Suzuki–Miyaura Coupling of Aryl Esters. *J. Am. Chem. Soc.* **2017**, *139*, 1311–1318. [[CrossRef](#)]
43. Torres Galvis, H.M.; Bitter, J.H.; Khare, C.B.; Ruitenbeek, M.; Dugulan, A.I.; de Jong, K.P. Supported Iron Nanoparticles as Catalysts for Sustainable Production of Lower Olefins. *Science* **2012**, *335*, 835–838. [[CrossRef](#)]
44. Ghogia, A.C.; Nzihou, A.; Serp, P.; Soulantica, K.; Pham Minh, D. Cobalt Catalysts on Carbon-Based Materials for Fischer-Tropsch Synthesis: A Review. *Appl. Catal. A Gen.* **2021**, *609*, 117906. [[CrossRef](#)]
45. Pedersen, E.Ø.; Svenum, I.H.; Blekkan, E.A. Mn Promoted Co Catalysts for Fischer-Tropsch Production of Light Olefins – An Experimental and Theoretical Study. *J. Catal.* **2018**, *361*, 23–32. [[CrossRef](#)]
46. Borji, F.; Pour, A.N.; Karimi, J.; Izadyar, M.; Keyvanloo, Z.; Hashemian, M. The Molecular Adsorption of Carbon Monoxide on Cobalt Surfaces: A DFT Study. *Prog. React. Kinet. Mech.* **2017**, *42*, 89–98. [[CrossRef](#)]
47. Yao, Z.; Guo, C.; Mao, Y.; Hu, P. Quantitative Determination of C–C Coupling Mechanisms and Detailed Analyses on the Activity and Selectivity for Fischer-Tropsch Synthesis on Co(0001): Microkinetic Modeling with Coverage Effects. *ACS Catal.* **2019**, *9*, 5957–5973. [[CrossRef](#)]
48. Chen, C.; Wang, Q.; Wang, G.; Hou, B.; Jia, L.; Li, D. Mechanistic Insight into the C₂ Hydrocarbons Formation from Syngas on Fcc-Co(111) Surface: A DFT Study. *J. Phys. Chem. C* **2016**, *120*, 9132–9147. [[CrossRef](#)]
49. Petersen, M.A.; Van Den Berg, J.A.; Ciobîcă, I.M.; Van Helden, P. Revisiting CO Activation on Co Catalysts: Impact of Step and Kink Sites from DFT. *ACS Catal.* **2017**, *7*, 1984–1992. [[CrossRef](#)]
50. Van Helden, P.; Van Den Berg, J.A.; Petersen, M.A.; Janse Van Rensburg, W.; Ciobîcă, I.M.; Van De Loosdrecht, J. Computational Investigation of the Kinetics and Mechanism of the Initial Steps of the Fischer-Tropsch Synthesis on Cobalt. *Faraday Discuss.* **2017**, *197*, 117–151. [[CrossRef](#)]
51. Ciobica, I.M.; van Rensburg, W.J. Hydrogen-Assisted CO Dissociation on FCC-Co {100}: DFT Analysis and Microkinetic Interpretation. In Proceeding of the EuropaCat IX, Catalysis for a Sustainable World, Salamanca, Spain, 30 August–4 September 2009.

52. Henkelman, G.; Uberuaga, B.P.; Jónsson, H. A Climbing Image Nudged Elastic Band Method for Finding Saddle Points and Minimum Energy Paths. *J. Chem. Phys.* **2000**, *113*, 9901–9904. [CrossRef]
53. Henkelman, G.; Jónsson, H. A Dimer Method for Finding Saddle Points on High Dimensional Potential Surfaces Using Only First Derivatives. *J. Chem. Phys.* **1999**, *111*, 7010–7022. [CrossRef]
54. Heyden, A.; Bell, A.T.; Keil, F.J. Efficient Methods for Finding Transition States in Chemical Reactions: Comparison of Improved Dimer Method and Partitioned Rational Function Optimization Method. *J. Chem. Phys.* **2005**, *123*, 224101. [CrossRef]
55. Kim, S.; Chen, J.; Cheng, T.; Gindulyte, A.; He, J.; He, S.; Li, Q.; Shoemaker, B.A.; Thiessen, P.A.; Yu, B.; et al. PubChem in 2021: New Data Content and Improved Web Interfaces. *Nucleic Acids Res.* **2021**, *49*, D1388–D1395. [CrossRef]
56. Bolton, E.E.; Chen, J.; Kim, S.; Han, L.; He, S.; Shi, W.; Simonyan, V.; Sun, Y.; Thiessen, P.A.; Wang, J.; et al. PubChem3D: A New Resource for Scientists. *J. Cheminform* **2011**, *3*, 32. [CrossRef]
57. National Center for Biotechnology Information. *PubChem Compound Summary*; National Center for Biotechnology Information: Bethesda, MD, USA, 2022.
58. NCBI National Center for Biotechnology Information. PubChem Substance Record for SID 10512399, HCOH (Hydroxymethylene) Source: NIST Chemistry WebBook. 2022. Available online: <https://pubchem.ncbi.nlm.nih.gov/substance/10512399> (accessed on 24 August 2022).
59. BIOVIA, Dassault Systèmes. *Materials Studio, 17.1.0.48*; Dassault Systèmes: San Diego, CA, USA, 2022.
60. Momma, K.; Izumi, F. VESTA 3 for Three-Dimensional Visualization of Crystal, Volumetric and Morphology Data. *J. Appl. Crystallogr.* **2011**, *44*, 1272–1276. [CrossRef]
61. Dubay, O.; Dubay, O. P4vasp. 2018. Available online: <http://Www.P4vasp.At/> (accessed on 20 August 2022).
62. Ganose, A.M.; Jackson, A.J.; Scanlon, D.O. Sumo: Command-Line Tools for Plotting and Analysis of Periodic Ab Initio Calculations. *J. Open. Source Softw.* **2018**, *3*, 717. [CrossRef]
63. Psfogiannakis, G.; St-Amant, A.; Ternan, M. Methane Oxidation Mechanism on Pt(111): A Cluster Model DFT Study. *J. Phys. Chem. B* **2006**, *110*, 24593–24605. [CrossRef]
64. Ashwell, A.P.; Lin, W.; Hofman, M.S.; Yang, Y.; Ratner, M.A.; Koel, B.E.; Schatz, G.C. Hydrogenation of CO to Methanol on Ni(110) through Subsurface Hydrogen. *J. Am. Chem. Soc.* **2017**, *139*, 17582–17589. [CrossRef] [PubMed]
65. Amaya-Roncancio, S.; Linares, D.H.; Duarte, H.A.; Sapag, K. DFT Study of Hydrogen-Assisted Dissociation of CO by HCO, COH, and HCOH Formation on Fe(100). *J. Phys. Chem. C* **2016**, *120*, 10830–10837. [CrossRef]
66. Zhu, Y.A.; Chen, D.; Zhou, X.G.; Yuan, W.K. DFT Studies of Dry Reforming of Methane on Ni Catalyst. *Catal. Today* **2009**, *148*, 260–267. [CrossRef]
67. Will Medlin, J.; Allendorf, M.D. Theoretical Study of the Adsorption of Acetylene on the (111) Surfaces of Pd, Pt, Ni, and Rh. *J. Phys. Chem. B* **2002**, *107*, 217–223. [CrossRef]
68. Zhang, M.; Dou, M.; Yu, Y. DFT Study of CO₂ Conversion on InZr₃(110) Surface. *Phys. Chem. Chem. Phys.* **2017**, *19*, 28917–28927. [CrossRef]
69. Hirunsit, P. Electroreduction of Carbon Dioxide to Methane on Copper, Copper–Silver, and Copper–Gold Catalysts: A DFT Study. *J. Phys. Chem. C* **2013**, *117*, 8262–8268. [CrossRef]
70. Liu, L.; Yao, H.; Jiang, Z.; Fang, T. Theoretical Study of Methanol Synthesis from CO₂ Hydrogenation on PdCu₃(111) Surface. *Appl. Surf. Sci.* **2018**, *451*, 333–345. [CrossRef]
71. Zhao, Y.F.; Yang, Y.; Mims, C.; Peden, C.H.F.; Li, J.; Mei, D. Insight into Methanol Synthesis from CO₂ Hydrogenation on Cu(1 1 1): Complex Reaction Network and the Effects of H₂O. *J. Catal.* **2011**, *281*, 199–211. [CrossRef]
72. Qi, Y.; Yang, J.; Duan, X.; Zhu, Y.A.; Chen, D.; Holmen, A. Discrimination of the Mechanism of CH₄ formation in Fischer-Tropsch Synthesis on Co Catalysts: A Combined Approach of DFT, Kinetic Isotope Effects and Kinetic Analysis. *Catal. Sci. Technol.* **2014**, *4*, 3534–3543. [CrossRef]
73. Cheng, J.; Hu, P.; Ellis, P.; French, S.; Kelly, G.; Martin Lok, C. Density Functional Theory Study of Iron and Cobalt Carbides for Fischer–Tropsch Synthesis. *J. Phys. Chem. C* **2009**, *114*, 1085–1093. [CrossRef]
74. Niu, J.; Du, X.; Ran, J.; Wang, R. Dry (CO₂) Reforming of Methane over Pt Catalysts Studied by DFT and Kinetic Modeling. *Appl. Surf. Sci.* **2016**, *376*, 79–90. [CrossRef]
75. Cheng, J.; Hu, P.; Ellis, P.; French, S.; Kelly, G.; Martin Lok, C. A First-Principles Study of Oxygenates on Co Surfaces in Fischer–Tropsch Synthesis. *J. Phys. Chem. C* **2008**, *112*, 9464–9473. [CrossRef]
76. Parr, R.G. Density Functional Theory. *Annu. Rev. Phys. Chem.* **1983**, *34*, 631–656. [CrossRef]
77. Orto, M.; Pantazis, D.A.; Neese, F. Density Functional Theory. *Photosynth. Res.* **2009**, *102*, 443–453. [CrossRef]
78. Cohen, A.J.; Mori-Sánchez, P.; Yang, W. Challenges for Density Functional Theory. *Chem. Rev.* **2012**, *112*, 289–320. [CrossRef]
79. Kresse, G.; Hafner, J. *Ab Initio* Molecular Dynamics for Liquid Metals. *Phys. Rev. B* **1993**, *47*, 558–561. [CrossRef] [PubMed]
80. Kresse, G.; Furthmüller, J. Efficient Iterative Schemes for *Ab Initio* Total-Energy Calculations Using a Plane-Wave Basis Set. *Phys. Rev. B* **1996**, *54*, 11169–11186. [CrossRef]
81. Kresse, G.; Hafner, J. *Ab Initio* Molecular Dynamics for Open-Shell Transition Metals. *Phys. Rev. B* **1993**, *48*, 13115–13118. [CrossRef] [PubMed]
82. Blöchl, P.E. Projector Augmented-Wave Method. *Phys. Rev. B* **1994**, *50*, 17953–17979. [CrossRef] [PubMed]
83. Kresse, G.; Joubert, D. From Ultrasoft Pseudopotentials to the Projector Augmented-Wave Method. *Phys. Rev. B* **1999**, *59*, 1758–1775. [CrossRef]

84. Perdew, J.P.; Burke, K.; Ernzerhof, M. Generalized Gradient Approximation Made Simple. *Phys. Rev. Lett.* **1996**, *77*, 3865–3868. [[CrossRef](#)]
85. Grimme, S.; Ehrlich, S.; Goerigk, L. Effect of the Damping Function in Dispersion Corrected Density Functional Theory. *J. Comput. Chem.* **2011**, *32*, 1456–1465. [[CrossRef](#)]
86. Henkelman, G.; Jónsson, H. Improved Tangent Estimate in the Nudged Elastic Band Method for Finding Minimum Energy Paths and Saddle Points. *J. Chem. Phys.* **2000**, *113*, 9978–9985. [[CrossRef](#)]
87. Olsen, R.A.; Kroes, G.J.; Henkelman, G.; Arnaldsson, A.; Jónsson, H. Comparison of Methods for Finding Saddle Points without Knowledge of the Final States. *J. Chem. Phys.* **2004**, *121*, 9776–9792. [[CrossRef](#)]
88. Kästner, J.; Sherwood, P. Superlinearly Converging Dimer Method for Transition State Search. *J. Chem. Phys.* **2008**, *128*, 014106. [[CrossRef](#)] [[PubMed](#)]
89. Xiao, P.; Sheppard, D.; Rogal, J.; Henkelman, G. Solid-State Dimer Method for Calculating Solid-Solid Phase Transitions. *J. Chem. Phys.* **2014**, *140*, 174104. [[CrossRef](#)] [[PubMed](#)]
90. Aroyo, M.I.; Orobengoa, D.; De La Flor, G.; Tasci, E.S.; Perez-Mato, J.M.; Wondratschek, H. Brillouin-Zone Database on the Bilbao Crystallographic Server. *Acta Crystallogr. A Found. Adv.* **2014**, *70*, 126–137. [[CrossRef](#)] [[PubMed](#)]
91. de la Peña O’Shea, V.A.; Moreira, I. de P.R.; Roldán, A.; Illas, F. Electronic and Magnetic Structure of Bulk Cobalt: The α , β , and ϵ -Phases from Density Functional Theory Calculations. *J. Chem. Phys.* **2010**, *133*, 024701. [[CrossRef](#)] [[PubMed](#)]
92. Hatzor, A.; Weiss, P.S. Molecular Rulers for Scaling Down Nanostructures. *Science* **2001**, *291*, 1019–1020. [[CrossRef](#)]
93. de la Peña O’Shea, V.A.; de la Piscina, P.R.; Homs, N.; Aromí, G.; Fierro, J.L.G. Development of Hexagonal Closed-Packed Cobalt Nanoparticles Stable at High Temperature. *Chem. Mater.* **2009**, *21*, 5637–5643. [[CrossRef](#)]
94. Sun, S.; Murray, C.B. Synthesis of Monodisperse Cobalt Nanocrystals and Their Assembly into Magnetic Superlattices (Invited). *J. Appl. Phys.* **1999**, *85*, 4325–4330. [[CrossRef](#)]
95. Materials Project. Available online: <https://materialsproject.org/> (accessed on 3 July 2022).
96. Liu, J.-X.; Su, H.-Y.; Sun, D.-P.; Zhang, B.-Y.; Li, W.-X. Crystallographic Dependence of CO Activation on Cobalt Catalysts: HCP versus FCC. *J. Am. Chem. Soc.* **2013**, *135*, 16284–16287. [[CrossRef](#)]
97. Skriver, H.L.; Rosengaard, N.M. Surface Energy and Work Function of Elemental Metals. *Phys. Rev. B* **1992**, *46*, 7157. [[CrossRef](#)] [[PubMed](#)]

Disclaimer/Publisher’s Note: The statements, opinions and data contained in all publications are solely those of the individual author(s) and contributor(s) and not of MDPI and/or the editor(s). MDPI and/or the editor(s) disclaim responsibility for any injury to people or property resulting from any ideas, methods, instructions or products referred to in the content.